



ISME

Cyclic Behavior of Beams Based on the Chaboche Unified Viscoplastic Model

V. Falahi *
M.Sc. Student

H. Mahbadi †
Associate Professor

M. R. Eslami ‡
Professor

In this paper, the ratcheting behavior of beams subjected to the mechanical cyclic loads at elevated temperature is investigated using the rate dependent Chaboche unified viscoplastic model with combined kinematic and isotropic hardening theory of plasticity. A precise and general numerical scheme, using the incremental method of solution, is developed to obtain the cyclic inelastic creep and plastic strains. Applying the numerical method to the equations obtained based on the mentioned unified model, the cyclic behavior of the beam due to the combined plastic and creep strains are obtained. Effect of loading rate, creep time, and mean load on ratcheting response and stress amplitude of the beam due to the combination of axial and bending moments at elevated temperature are obtained. It is shown that that increasing the loading rate, results to decrease in ratcheting rate and increase in stress amplitude. Also the ratcheting strain increases with increasing the creep time while the stress amplitude decreases. The results obtained using the applied method in this paper is verified with the experimental data given in the literature search.

Keywords: Cyclic loading, Rate dependent plasticity, Creep, Viscoplasticity, Load controlled, Strain controlled

1 Introduction

Structural problems under mechanical and thermal cyclic loadings are frequently encountered in the design problems. The applied external load may be high enough to bring the structure into the plastic range. The question remains in the true behavior of a structure in regard to the shake-down or ratcheting and, in the latter case, the number of cyclic loads that the structure stands before failure. In special cases, where the material is under high temperature environment, understanding of the material behavior under cyclic loading condition for lifetime prediction is important.

Many criteria and models are proposed in literature to estimate the behavior of a structure under cyclic loading condition. In (1986) J. L. Chaboche [1] proposed a time independent constitutive model for cyclic plasticity which is included non-linear kinematic hardening theory with isotropic hardening theory that is capable to estimate consequences of cyclic loading much

* M.Sc. Student, Department of Mechanical Engineering, Amirkabir University of Technology, Tehran, Iran, vahid-falahi@aut.ac.ir

† Corresponding Author, Associate Professor, Department of Mechanical Engineering, Central Tehran Branch, Islamic Azad University, Tehran, Iran, h_mahbadi@iauctb.ac.ir

‡ Professor and Fellow of the Academy of Sciences, Department of Mechanical Engineering, Amirkabir University of Technology, eslami@aut.ac.ir

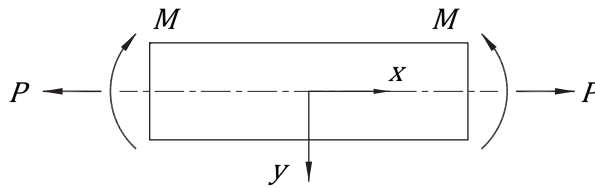


Figure 1 Geometry and loading of the beam.

accurately than previous linear kinematic hardening and non-combined models. In the past decades a several viscoplasticity constitutive models are proposed to predict the structural behavior under cyclic loading at high elevated temperatures. In (1983), Chaboche [2, 3] proposed the unified viscoplastic constitutive model. In this model, the kinematic and isotropic hardening theories are considered in a unified form. Contrary to 1986 Chaboche model this theory is a time dependent model which is able to evaluate effects of rate and creep time and also it is suitable for high temperature conditions which effects of rate are crucial. This model is widely accepted in literature. The key problem to properly use this model is how to select the initial set of the material properties which are used in the model. This problem is resolved and referred in literature by a number of authors such as Tong et al. [4], Zhan [5], Mahnken and Stein [6], Schwertel and Schinke [7], Fossum [8, 9], and Gong and Hyde and Sun [10]. There are also another viscoplastic constitutive models using nonlinear Armstrong Frederick [11] kinematic hardening theory as Walker [12], Moreno and Jordan [13], ohno [14, 15], Lee and Krempl [16].

The authors have been studied the cyclic loading of beams based on the non-unified version of Chaboche constitutive model which is a rate independent model [17]. In this study, the Chaboche unified viscoplastic model [1, 2, 3, 18, 19] is considered, which is a time dependent model with combined kinematic and isotropic hardening theory. The model allows to reasonably predict the behavior of materials under cyclic loading condition. The assumed beam material is considered to be type 316 stainless steel, where to obtain the coefficients and parameters of the material for starting point of cyclic loading, reference [10] is used. The numerical analysis is carried out using the experimental results of type 316 stainless steel. Loading is assumed under isothermal condition at temperature 500 °C. Due to the nonlinearity of the problem and applying the combined isotropic and kinematic hardening theory of plasticity including a model wherein the plastic and creep strains are obtained by a unified flow rule, a numerical method is proposed to solve the coupled and stiff differential equations of the problem. This numerical method is the modification of the method which is proposed by Mahbadi and Eslami [20, 21, 22, 23, 17]. The novelty of present study, in comparison to the published papers reported on cyclic loading of beams, is application of a time dependent constitutive model to obtain both of the plastic and creep strains due to the combination of axial and bending loads in isothermal condition. Applying this model results to evaluating the effect of loading rate and creep time on ratcheting behavior of the beam.

2 Mathematical Formulation

A beam with rectangular cross section is considered, as shown in Fig. (1). The beam is made of isotropic materials with height of $2c$ and width of h and subjected to the combination of axial load and bending moment, as shown in this figure. The total axial mechanical strain of the beam is obtained by adding the elastic and inelastic strains as follows

$$\epsilon_x = \frac{\sigma_x}{E} + \epsilon_x^p + \epsilon_x^{Res} \quad (1)$$

In Eq. (1), the axial stress, inelastic strain (i.e. including creep and plastic strains), and the residual strain are represented with σ_x , e_x^p and e_x^{Res} , respectively. The elastic modulus is E and the parameters are normalized for convergency of the numerical method as

$$S = \frac{\sigma_x}{\sigma_0}, \quad e_x = \frac{\epsilon_x}{\epsilon_0}, \quad e_x^p = \frac{\epsilon_x^p}{\epsilon_0}, \quad e_x^{Res} = \frac{\epsilon_x^{Res}}{\epsilon_0}, \quad \eta = \frac{y}{c} \quad (2)$$

In this equation, σ_0 and ϵ_0 are the initial yield stress and yield strain, respectively, and y is layers distance to the beam neutral axis. The dimensionless form of the compatibility equation is used to obtain the axial strain as

$$\frac{\partial^2 e_x}{\partial \eta^2} = 0 \longrightarrow e_x = c_1 + c_2 \eta \quad (3)$$

In Eq. (3) c_1 and c_2 are constants of integration and are defined using the equilibrium condition of the beam. Substituting e_x from Eq. (3) into the normalized form of Eq. (1) and solving for S gives

$$S = c_1 + c_2 \eta - e_x^p - e_x^{Res} \quad (4)$$

Thus, the equilibrium condition of the beam due to imposed axial load P and moment M results in

$$\begin{aligned} P^* &= \int_{-1}^1 S d\eta = \frac{P}{\sigma_0 c h} \\ M^* &= \int_{-1}^1 S \eta d\eta = \frac{P}{\sigma_0 c^2 h} \end{aligned} \quad (5)$$

The constants of integration are found by substituting Eq. (4) into Eqs. (5) as follow

$$\begin{aligned} c_1 &= \frac{P^*}{2} + \frac{1}{2} \int_{-1}^1 e_x^p d\eta + \frac{1}{2} \int_{-1}^1 e_x^{Res} d\eta \\ c_2 &= \frac{3}{2} M^* + \frac{3}{2} \int_{-1}^1 e_x^p \eta d\eta + \frac{3}{2} \int_{-1}^1 e_x^{Res} \eta d\eta \end{aligned} \quad (6)$$

Upon substitution, the dimensionless stress distribution in the cross section of the beam is obtained as

$$\begin{aligned} S &= \frac{P^*}{2} + \frac{1}{2} \int_{-1}^1 e_x^p d\eta + \frac{1}{2} \int_{-1}^1 e_x^{Res} d\eta + \eta \left[\frac{3}{2} M^* + \frac{3}{2} \int_{-1}^1 e_x^p \eta d\eta \right. \\ &\quad \left. + \frac{3}{2} \int_{-1}^1 e_x^{Res} \eta d\eta \right] - e_x^p - e_x^{Res} \end{aligned} \quad (7)$$

and the axial dimensionless strain is

$$\begin{aligned} e_x &= \frac{P^*}{2} + \frac{3}{2} \eta M^* + \frac{1}{2} \int_{-1}^1 e_x^p d\eta + \frac{1}{2} \int_{-1}^1 e_x^{Res} d\eta + \frac{3}{2} \eta \int_{-1}^1 e_x^p \eta d\eta \\ &\quad + \frac{3}{2} \eta \int_{-1}^1 e_x^{Res} \eta d\eta \end{aligned} \quad (8)$$

3 Unified Viscoplastic Constitutive Model

The viscoplastic constitutive equations which are proposed by Chaboche [2] for inclusion of time or strain rate using a von Mises criterion and normality rule is

$$d\epsilon_{ij}^p = \frac{3}{2} \left\langle \frac{J(\sigma_{ij} - \chi_{ij}) - R - \sigma_0}{Z} \right\rangle^n \frac{\sigma'_{ij} - \chi'_{ij}}{J(\sigma_{ij} - \chi_{ij})} dt \quad (9)$$

The yield criterion for the material which the above constitutive model is associated with, is

$$f = J(\sigma_{ij} - \chi_{ij}) - R - \sigma_0 \quad (10)$$

The McCauley bracket $\langle \cdot \rangle$ is used here to ensure that when $f < 0$, the state of stress is inside the elastic domain. In equations (9) and (10), χ_{ij} is the backstress tensor, n and Z are material constants, R is associated parameter to the isotropic hardening of material and is recalled as drag stress, σ'_{ij} and χ_{ij} are deviatoric stress and back stress tensors and J represents a distance in the stress space which for von Mises yield criterion is

$$J(\sigma_{ij} - \chi_{ij}) = \left[\frac{3}{2} (\sigma'_{ij} - \chi'_{ij})(\sigma'_{ij} - \chi'_{ij}) \right]^{1/2} \quad (11)$$

The backstress tensor χ_{ij} corresponding to this viscoplastic yield criterion is defined as

$$d\chi_{ij} = d\chi_{ij}^{(1)} + d\chi_{ij}^{(2)} \quad (12)$$

wherein

$$d\chi_{ij}^{(1)} = C_1 (a_1 d\epsilon_{ij}^p - \chi_{ij}^{(1)} d\epsilon_p) \quad (13)$$

$$d\chi_{ij}^{(2)} = C_2 (a_2 d\epsilon_{ij}^p - \chi_{ij}^{(2)} d\epsilon_p) \quad (14)$$

The parameters C_1 , C_2 , a_1 , and a_2 are material constants for the Chaboche kinematic hardening model and are obtained from the uniaxial test. The equivalent plastic strain $d\epsilon_p$ is

$$d\epsilon_p = \left(\frac{2}{3} d\epsilon_{ij}^p d\epsilon_{ij}^p \right)^{1/2} = \left\langle \frac{J(\sigma_{ij} - \chi_{ij}) - R - \sigma_0}{Z} \right\rangle^n \quad (15)$$

For load or strain controlled cyclic loading with approximately constant strain cycling, drag stress R is defined as

$$dR = b(Q - R)d\epsilon_p \quad (16)$$

Defining the following normalized parameters,

$$\begin{aligned} \bar{\chi} &= \frac{\chi}{\sigma_0}, & \bar{C}_k &= \frac{C_k}{E}, & \bar{a} &= \frac{a}{\sigma_0}, & \bar{f} &= \frac{f}{\sigma_0} \\ \bar{R} &= \frac{R}{\sigma_0}, & \bar{Z} &= \frac{Z\epsilon_0^{1/n}}{\sigma_0}, & \bar{Q} &= \frac{Q}{\sigma_0}, & \bar{b} &= \frac{b\sigma_0}{E} \end{aligned} \quad (17)$$

the model for uniaxial loading is normalized as follow

Normalized yield criterion:

$$\bar{f} = |S - \bar{\chi}| - \bar{R} - 1 \quad (18)$$

Constitutive model:

$$de_x^p = \left\langle \frac{\bar{f}}{\bar{Z}} \right\rangle^n \text{sgn}(S - \bar{\chi}) \quad (19)$$

Equivalent plastic strain (or experimental stress strain curve):

$$de_p = \left\langle \frac{\bar{f}}{\bar{Z}} \right\rangle^n \quad (20)$$

Axial component of back stress tensor:

$$d\bar{\chi}_x = \sum_{k=1}^2 \bar{C}_k (\bar{a}_k de_x^p - \bar{\chi}_x d\bar{e}_p) \quad (21)$$

and drag stress:

$$d\bar{R} = \bar{b}(\bar{Q} - \bar{R})d\bar{e}_p \quad (22)$$

4 Numerical Solution

In this section, the numerical solution procedure for plastic analysis and cyclic loading behavior of beams under mechanical and thermal loads is described. The numerical method described by Mahbadi and Eslami [24] is developed for viscoplastic material to solve the problem. Due to history dependency and nonlinearity of inelasticity problems, the proposed numerical method is based on an incremental iterative method. This method is proposed applying the successive coordinate systems corresponding to each cycle during the loading and unloading procedure, as shown in Fig. (2). The solution obtained in these successive coordinate systems is transferred to the main coordinate system located at the beginning of the first cycle of load. Thus, the coordinate system corresponding to the first cycle of the load is identical with the main coordinate system. When the number of cycles are increased, the subsequent successive coordinate systems differ with the main coordinate system. The problem is solved in each successive coordinate system independently while the parameters such as back stress and residual stresses are initialized based on the results obtained in previous coordinate system and transferred to the current coordinate system according to proper coordinate transformation. The detail of the method is described in following steps:

- Step 1: Using Eqs. (5), the axial force and bending moment are normalized and the yield load, or the critical load, is specified. Further loads result into plastic deformation of a section of the beam. The additional applied load, the final load minus the critical yielding load, is divided into N equal divisions. Also, divide the beam cross section across its thickness into m layers. All the input variables are initialized and normalized. The initial data for each layer of the beam across its thickness is set from the elasticity solution and the plastic strains of all layers are set to zero. The yield stress k for the first cycle is the value of initial yield stress.
- Step 2: The load is advanced one step and the induced stresses in each layer are calculated using Eq. (7).
- Step 3: For each layer, the yield criteria from Eq. (18) is checked to determine if the layer is in plastic zone. For the layers that are in plastic range, a value for the plastic strain increment Δe_p is assumed and is added to the accumulated plastic strain from previous step of loading (i.e. for the first increment of plastic strain the accumulated plastic strain is zero) to obtain the total plastic strain.

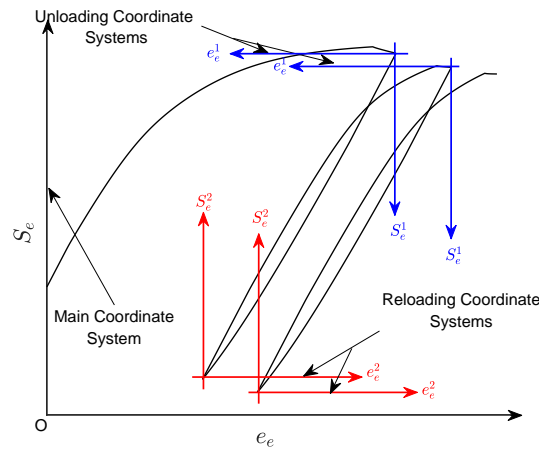


Figure 2 Subsequent coordinate systems.

- Step 4: The value of plastic strain for each layer is substituted into Eq. (7) to obtain the axial stress for each layer. To calculate the integral functions of e_x^p one may use any numerical integration method [24]. As a typical method, the trapezoidal method may be used as follows:

$$\int_a^b f(e_{ij}^p(\rho))d\rho = \frac{\Delta\eta}{2}[f(e_{ij}^p(a)) + 2\sum_{k=2}^{\rho-1}f(e_{ij}^p(\rho_k)) + f(e_{ij}^p(b))] \quad (23)$$

- Step 5: Increments of back stress and drag stress are obtained using Eqs. (21) and (22).
- Step 6: A new value for equivalent plastic strain is obtained using the experimental stress strain curve shown in Eq. (20).
- Step 7: a new value for axial plastic strain increment is obtained using Eq. (19).
- Step 8: Steps 3 through 7 are repeated until the increment of plastic strain Δe_p converges.
- Step 9: The steps 2 through 8 are repeated up to the final amount of load.
- Step 10: For unloading, a second coordinate system in reverse direction is mounted at the current state of stress and strain values.
- Step 11: All the values of stress, strain, accumulated and total plastic strains are set to zero. The values for back stress and drag stress are transferred to the unloading coordinate system as follow:

$$\bar{\chi}_x^{acc} = S_x^2 - \bar{\chi}_x \quad (24)$$

$$\bar{R}^{acc} = \bar{R} \quad (25)$$

where $\bar{\chi}_x^{acc}$ and \bar{R}^{acc} are the accumulated back stress and drag stress in unloading coordinate system and S_x^2 is the maximum value of axial stress in previous loading system.

- Step 12: Steps 2 through 9 are repeated for unloading procedure until the maximum value of load is achieved. It should be mentioned that the maximum unload value is difference between the absolute values of maximum and minimum loads which the load is cycled.

Also, the total stress and strain are transferred into the main coordinate system using the following equations:

$$\begin{aligned} S_x &= S_x^0 - S_x^1 \\ e_x &= e_x^0 - e_x^1 \\ e_x^p &= e_x^{p0} - e_x^{p1} \end{aligned} \quad (26)$$

where superscript 1 show the values corresponding to the unloading coordinate system and superscript 0 shows the values corresponding to the previous loading at maximum load in main coordinate system.

- Step 13: For reloading, a third coordinate system is attached to the current state of stress and strain values in the same direction of the main coordinate system.
- Step 14: All values of stress, strain, accumulated, and total plastic strains are set to zero. The values for back stress and drag stress are transferred into the reloading coordinate system as:

$$\bar{\chi}_x^{acc} = S_x^1 - \bar{\chi}_x \quad (27)$$

$$\bar{R}^{acc} = \bar{R} \quad (28)$$

where $\bar{\chi}_x^{acc}$ and \bar{R}^{acc} are the accumulated back stress and drag stress in reloading coordinate system and S_x^1 is the maximum value of axial stress in previous unloading system.

- Step 15: Steps 2 through 9 are repeated for reloading procedure until the maximum value of load is achieved. Also, the total stress and strain are transferred into the main coordinate system using the following equations:

$$\begin{aligned} S_x &= S_x^0 + S_x^2 \\ e_x &= e_x^0 + e_x^2 \\ e_x^p &= e_x^{p0} + e_x^{p2} \end{aligned} \quad (29)$$

where superscripts 2 show the values corresponding to the reloading coordinate system.

- Step 16: Procedure between steps 2 through 15 is repeated until the final cycle of load is archived.

The flow chart of the above numerical procedure has been shown in Figure (3).

5 Results and Discussion

In this section the effect of creep on load and strain controlled cyclic loading of beam structure is investigated. For the following examples, a beam made of SS316 steel is considered. The cross section of the beam is rectangular with height $2c = 50$ mm and width $h = 25$ mm. The geometry, elastic, plastic, and typical values for creep properties of the beam are given in Table (1) [10].

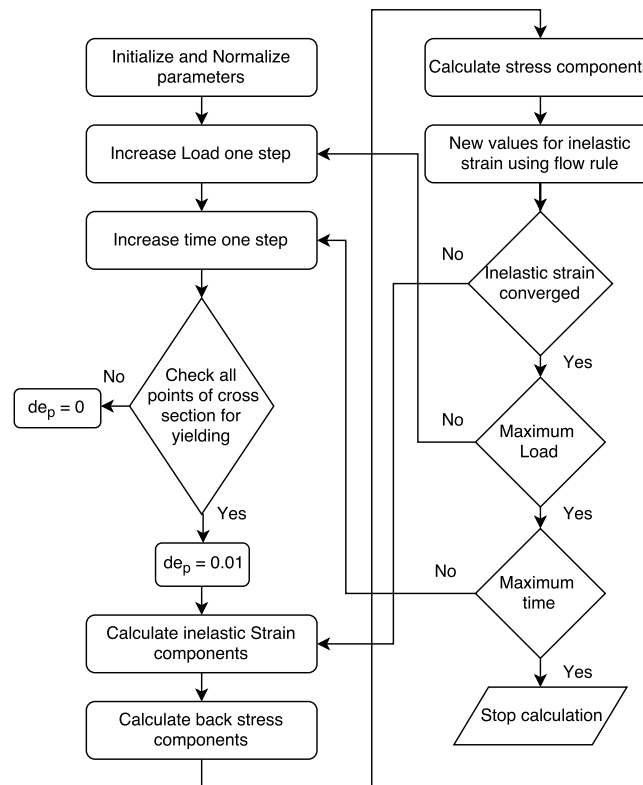


Figure 3 Flow chart of numerical procedure

Table 1 Optimized material constant at 500 °C temperature [10].

Properties	Notation	Value	Unit
Initial Yield Stress	σ_0	37.98	MPa
Modules of Elasticity	E	135.4666	GPa
Isotropic Hardening Parameter	B	16.77	-
Isotropic Hardening Parameter	Q	32.79	MPa
Kinematic Hardening Parameter	a_1	36.66	MPa
Kinematic Hardening Parameter	C_1	19963.66	-
Kinematic Hardening Parameter	a_2	160.59	MPa
Kinematic Hardening Parameter	C_2	1506.58	-
Creep Law Parameter	Z	70.60	MPa · s ^{1/n}
Creep Law Parameter	n	40.00	-

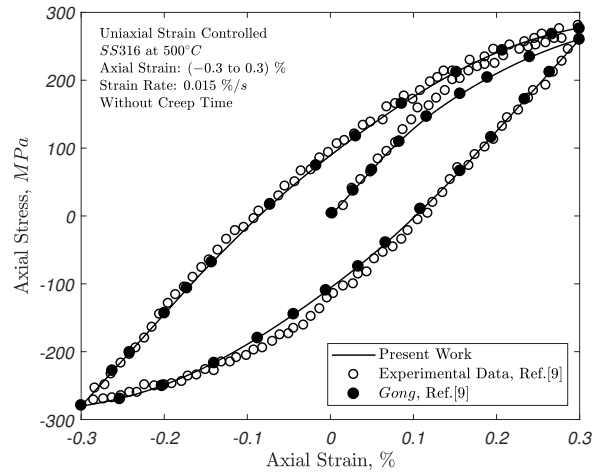


Figure 4 Comparison of 1st load cycle with the experimental data of Ref. [10].

5.1 Comparison of Model and Experimental Data

In Figs. (4) through (7), the numerical results obtained in present work are compared with experimental data for a rectangular steel beam with material properties given in Table (1). Figure (4) shows the comparison between the results obtained in present work and the experimental data of Gong [10] under deformation controlled condition and uniform temperature 500°C for the first cycle of loading. The axial strain is cycled between -0.3% and 0.3% and the strain rate which is used to evaluate the results is $\dot{\varepsilon}_x = 0.015\%/s$. As the figure shows, the numerical results are in close agreement with the experimental data and the percentage of error at the end of loading and unloading is approximately 3% . Figure (5) shows the stabilized hysteresis loop at 50^{th} cycle in comparison with the experimental data and the difference between the axial strain obtained in this work and experimental data at -0.3% and 2.4% is about 0.3% and 4.8% respectively. Fig. (6) shows the amplitude of stress versus the number of cycles up to the stabilized hysteresis loop represented in the previous figure. The results between the proposed method and the experimental data are well compared and percentage of error in the first cycle is about 1.2% and in the 50^{th} cycle is just 0.34% . The maximum error occurs in 22^{th} cycle which is 1.7% .

In the next example, a beam made of Nickel based alloy under axial cyclic deformation is cycled through $\varepsilon_x = -1$ to 1% with $20s$ relaxation time at the end of per half cycle. The material properties of the beam are: elasticity modulus $E = 170\text{GPa}$, yield stress $\sigma_0 = 144.26\text{MPa}$, kinematic hardening parameters $C_1 = 391.61$, $C_2 = 2578.69$, $a_1 = 361.57\text{MPa}$, $a_2 = 26.84\text{MPa}$, isotropic hardening parameters $Q = 161.52\text{MPa}$, $b = 5.54$ and the viscoplastic parameters $n = 15.496$, $z = 678.317\text{MPa} \cdot s^{\frac{1}{n}}$. Figure (7) shows that the experimental data of Ref. [4] and numerical data of current work are in close agreement and the maximum error between the present work and experimental data is about 6% .

5.2 Axial loading

In Figs. (8) through (11) axial stress versus the axial strain are plotted to show the effect of mean load and creep time on cyclic response of the beam made of material properties given in Table (1) at 500°C . In Figs. (8), (9), and (10) the axial load is cycled between -300 and 300KN wherein the mean load is zero. In Fig. (8), creep time is not included at the end of both loading and unloading half cycles and reversed plasticity behavior is observed. In Fig. (9), the creep is

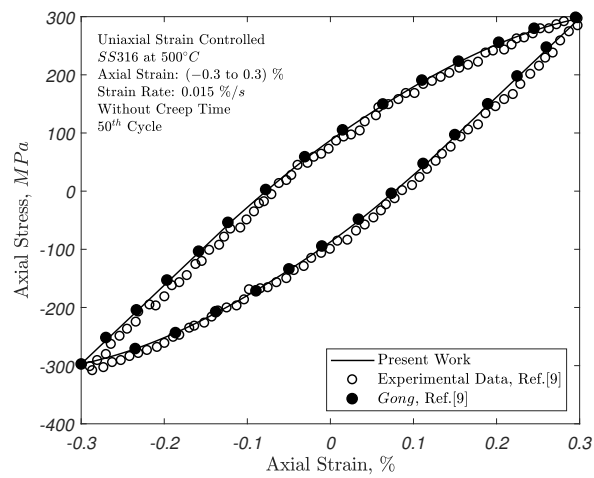


Figure 5 Comparison of 50th load cycle with the experimental data of Ref. [10].

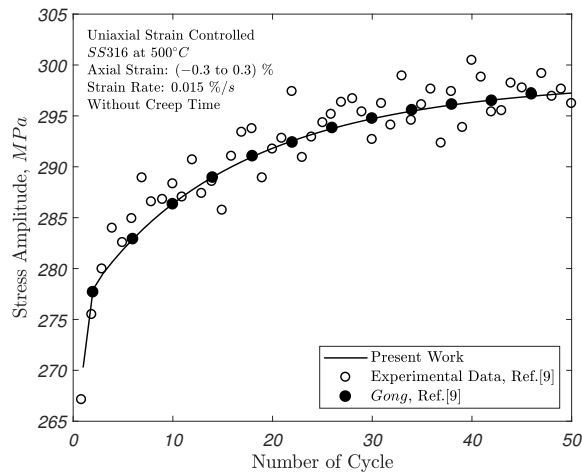


Figure 6 Comparison of stress amplitude with the experimental data of Ref. [10].

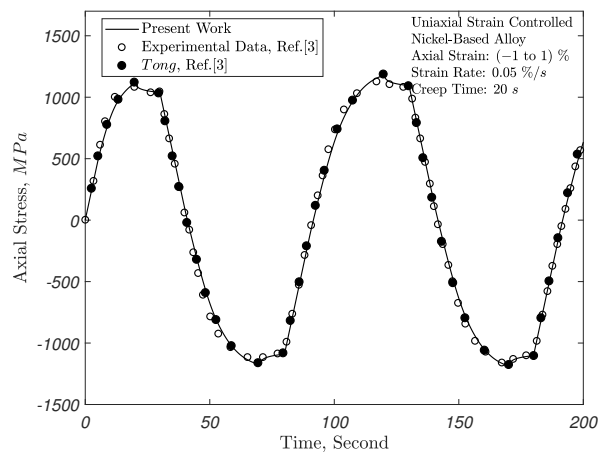


Figure 7 Comparison with experimental data of Ref. [4].

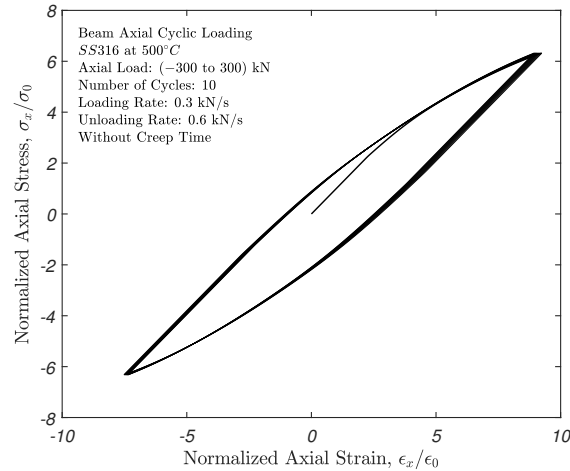


Figure 8 Reversed plasticity due to the axial cyclic loading with zero mean load.

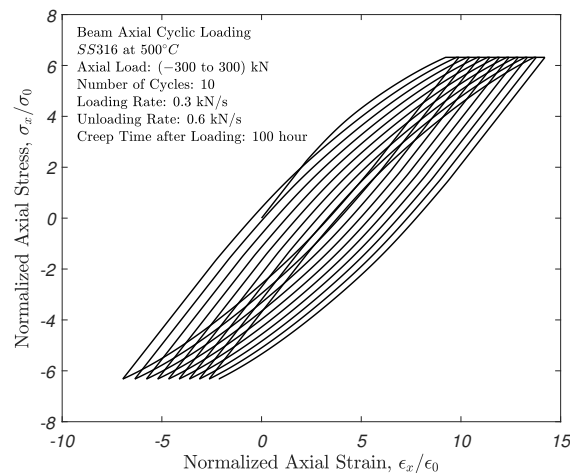


Figure 9 Ratcheting due to the creep on loading half cycles.

considered only at the end of loading cycle and ratcheting behavior is observed. In Fig. (10), creep is included at the end of both loading and unloading half cycles and reversed plasticity is observed. The creep time at the end of loading or unloading half cycles is 100hr in Figs. (9) and (10).

Figures (11) and (12) show the cyclic loading results of the beam with nonzero axial mean load. In these figures the axial load is cycled between -200 to 300KN . The plot of axial stress versus the axial strain in Fig. (11) shows the ratcheting behavior for the case which the creep time is excluded. The plot of peak strain at the end of each loading half cycle in Fig. (12) represents the effect of creep time at the end of half cycles on ratcheting rate of the beam. As the figure shows, the highest ratcheting rate is archived for the case which the creep time is included only at the end of loading half cycle while the minimum strain rate is obtained for the case which excludes the creep effect.

5.3 Bending moment loading

The cyclic loading behavior of the beam due to the bending moment is studied in this part. When the beam is subjected to the zero mean load, the same behavior of the beam due to the axial load

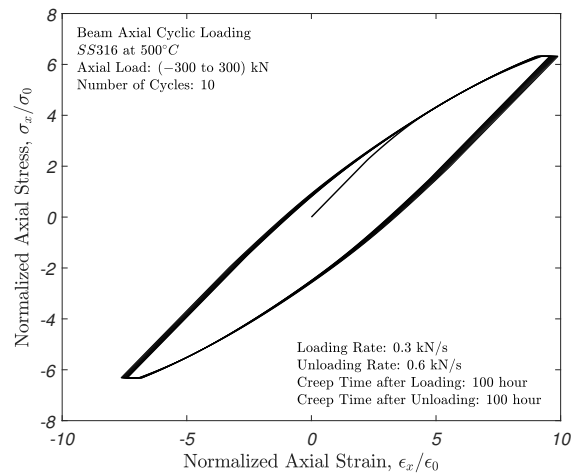


Figure 10 Reversed plasticity due to the axial cyclic loading including the creep.

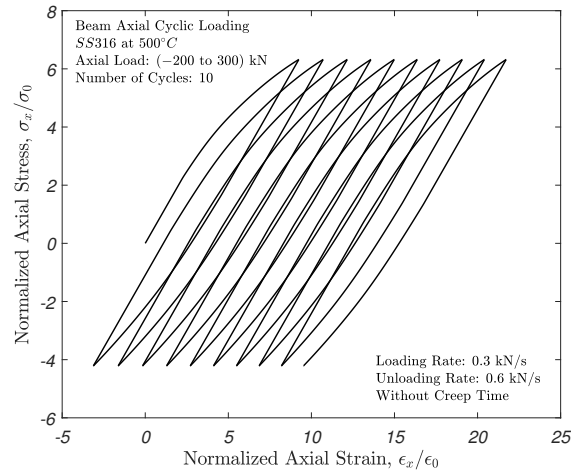


Figure 11 Ratcheting due to the nonzero axial mean load.

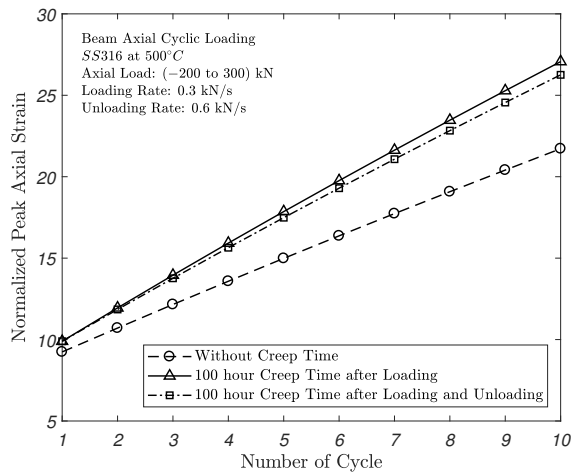


Figure 12 Effect of creep on ratchetting of axially loaded beam.

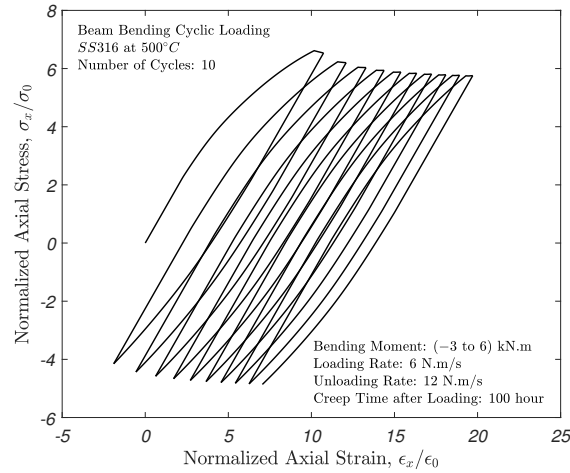


Figure 13 Bending moment with non-zero mean load and creep after the loading half cycle.

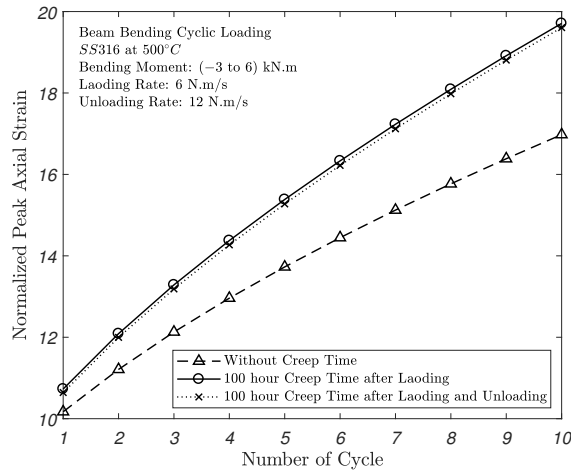


Figure 14 Effect of creep time on ratcheting of the beam subjected to the bending moment.

is achieved but the results are not shown here. That is, the ratcheting behavior is achieved when the creep is considered at the end of each half load cycle and excluded during the half unloading cycles. Figures (13) and (14) show the response of the beam at its top layer due to the cyclic bending moment with nonzero mean load. The bending moment in these figures is cycled between $-3KN.m$ and $6KN.m$. The figures show the same ratcheting behavior of the beam obtained for the axial load except that the maximum stress will decrease in first few load cycles. In these figures the loading rate is assumed to be $12 N.m/s$. Figure (15) shows that the lowest stress amplitude corresponds to the case where the creep time is considered at the end of both loading and unloading half cycles while the maximum stress amplitude corresponds to the case which the creep is considered at the end of loading half cycle.

Figures (16) and (17) investigate the effect of loading rate on ratcheting response and stress amplitude of the beam subjected to the cyclic bending moment. In these figures, the bending moment is cycled between -3 and $6 KN.m$. Figure (16) shows that increasing the loading rate results to decrease in ratcheting rate of the beam while the stress amplitude increases with increasing the loading rate, as shown in Fig. (17)

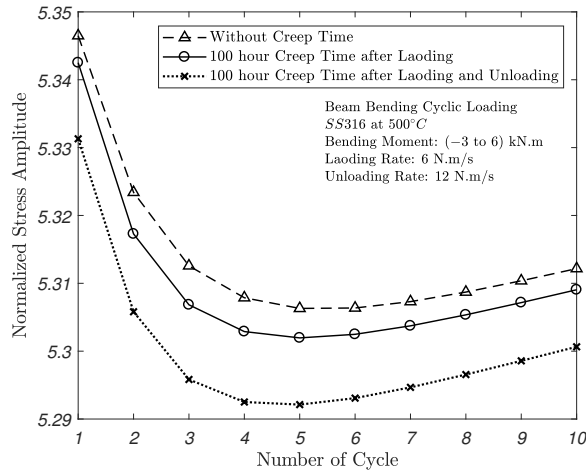


Figure 15 Variation of stress amplitude of the beam subjected to the bending moment.

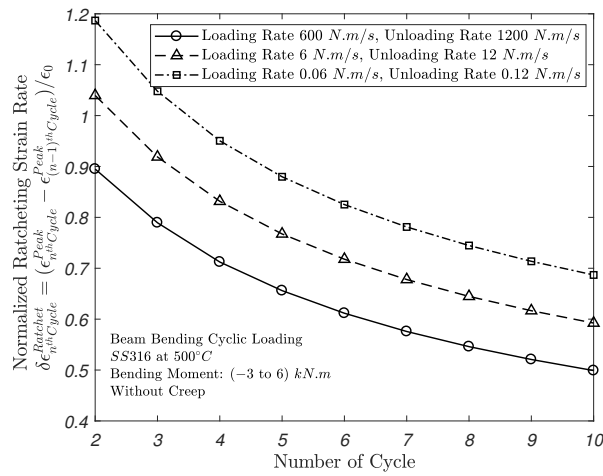


Figure 16 Beam cyclic loading under bending moment with non-zero mean load without creep time in different loading rate.

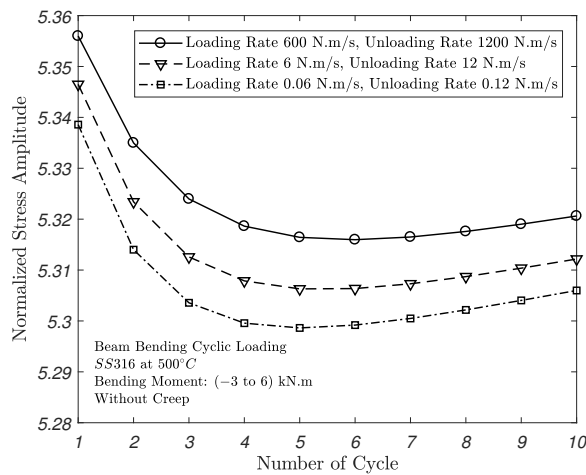


Figure 17 Beam cyclic loading under bending moment with non-zero mean load without creep time in different loading rate.

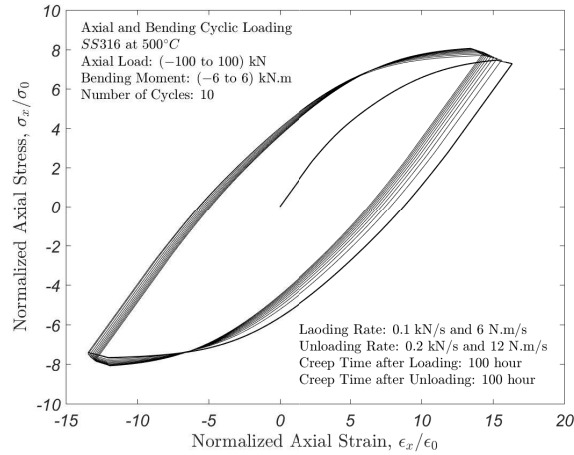


Figure 18 Combined axial and bending moment cyclic loading with symmetric loading and loading condition.

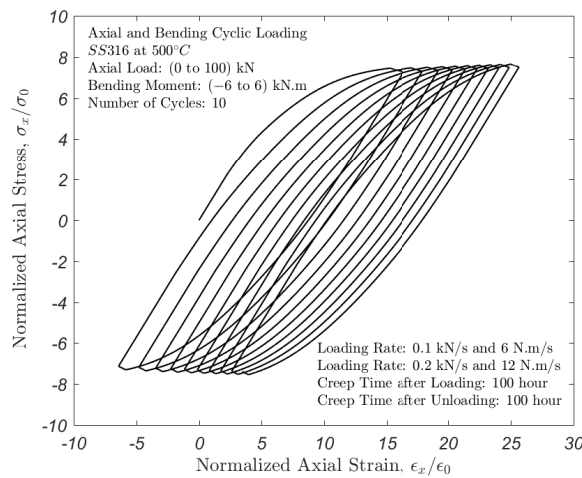


Figure 19 Combined axial and bending moment cyclic loading with unsymmetric loading and loading condition.

5.4 Combined loading

In Figs. (18) through (19), cyclic loading behavior of the beam subjected to the combination of axial load and bending moment is investigated. When the beam is subjected to the proportional cyclic axial and bending moment with zero mean load, identical loading/unloading rate and identical creep conditions at the end of both loading and unloading half cycle, the beam shows reversed plasticity behavior. This behavior is represented in Fig. (18) for top and bottom layers of the beam and under cyclic axial load -100 to 100 KN and cyclic bending moment -6 to 6 $KN.m$. When the conditions used for Fig. (18) are not available, the symmetry condition during loading and unloading is removed and ratcheting behavior is observed as the result of cyclic loading. This behavior is shown in Fig. (19) for the case which mean axial load is not zero. In this figure the axial load is cycled between 0 and 100 KN , the bending moment is cycled between -6 to 6 $KN.m$, the loading rate for axial load and bending moment is 0.1 KN/s and 6 $N.m/s$, respectively, while the unloading rate is 0.2 KN/s and 12 $N.m/s$, respectively.

6 Conclusion

Applying the compatibility and equilibrium equations, equations are obtained for stress and strain distribution along the height of a beam subjected to the axial and bending moment loads. A unified Chaboche viscoplastic model with combined isotropic and kinematic hardening theories is used to evaluate the inelastic strains at elevated temperature. A numerical method is proposed which is quiet capable and efficient to handle the cyclic loading analysis of the viscoplastic structures. Cyclic response of a beam due to the axial loading, bending moment loading, and combined axial and bending moment loading is studied employing the proposed numerical method. The effect of mean load, creep time, loading rate on ratcheting or reversed plasticity behavior of the beam subjected to the mentioned mechanical load is obtained at elevated temperatures. The simulation results show that when the beam is subjected to symmetric loading and unloading conditions, cyclic loading of the beam results to reversed plasticity. When either the creep time or the loading rate are not equal in loading and unloading conditions, ratcheting behavior is obtained due to the cyclic loading of beams. When the mean load is not zero, ratcheting behavior is obtained in all loading conditions. On the other hand, the represented data show that increasing the loading rate results to decrease in ratcheting rate, while increasing the creep time results to increase in ratcheting rate. When the beam is subjected to bending moment, increase in loading rate results to increase in stress amplitude while the stress amplitude decreases with increasing the creep time.

References

- [1] Chaboche, J.L., "Time Independent Constitutive Theories for Cyclic Plasticity", *International Journal of Plasticity*, Vol. 32, No. 2, pp. 149-188, (1986).
- [2] Chaboche, J.L., and Rousselier, G., "On the Plastic and Viscoplastic Constitutive Equations Part 1: Rules Developed with Internal Variable Concept", *Journal of Pressure Vessel Technolgy*, Vol. 105, No. 2, pp. 153-158, (1983).
- [3] Chaboche, J.L., and Rousselier, G., "On the Plastic and Viscoplastic Constitutive Equations Part 2: Application of Internal Variable Concepts to the 316 Stainless Steel", *Journal of Pressure Vessel Technolgy*, Vol. 105, No. 2, pp. 159-164, (1983).
- [4] Tong, J., Zhan, Z.L., and Vermeulen, B., "Modelling of Cyclic Plasticity an Viscoplasticity of a Nickel-Based Alloy using Chaboche Constitutive Equations", *International Journal of Fatigue*, Vol. 26, No. 8, pp. 829-837, (2004).
- [5] Zhan, Z., "A Study of Creep-Fatigue Interaction in a New Nickel-Based Superalloy", PhD Theis, University of Portsmouth, UK, (2004).
- [6] Mahnken, Z., and Stein, E., "Parameter Identification for Viscoplastic Model Based on Analytical Derivatives of a Least-Squares Functional and Stability Investigations", *International Journal of Plasticity*, Vol. 12, No. 4, pp. 451-479, (1996).
- [7] Schwertel, J., and Schinke, B., "Automated Evaluation of Material Parameters of Viscoplastic Constitutive Equations", *Transactions of ASME, Journal of Engineering Materials Technolgy*, Vol. 118, No. 3, pp. 273-280, (1996).

- [8] Fossum, A.F., "Parameter Estimation for an Internal Variable Model using Nonlinear Optimization and Analytical/Numerical Response Sensitivities", *Transactions of ASME, Journal of Engineering Materials Technology*, Vol. 119, No. 4, pp. 337-345, (1997).
- [9] Fossum, A.F., "Rate Data and Material Parameter Estimation", *Transactions of ASME, Journal Engineering Materials and Technology*, Vol. 120, No. 1, pp. 7-12, (1998).
- [10] Gong, Y.P., Hyde, C.J., Sun, W., and Hyde, T.H., "Determination of Material Properties in the Chaboche Unified Viscoplasticity Model", *Journal of Materials Design and Applications*, Vol. 224, No. 1, pp. 19–29, (2010).
- [11] Frederick, C.O., and Armstrong, C.O., "A Mathematical Representation of the Multiaxial Bauschinger Effect", *Materials at High Temperatures*, Vol. 24, No. 1, pp. 1–26, (2007).
- [12] Walker, K.P., "Research and Development Program for Non-Linear Structural Modeling with Advanced Time-Temperature Dependent Constitutive Relationships", Technical Report 19820008207, NASA, United Technologies Research Center; East Hartford, CT, United States, Nov. 25, (1981).
- [13] Moreno, V., and Jordan, E.H., "Prediction of Material Thermomechanical Response with a Unified Viscoplastic Constitutive Model", *International Journal of Plasticity*, Vol. 2, No. 3, pp. 223–245, (1986).
- [14] Murakami, S., and Ohno, N., "A Constitutive Equation of Creep Based on the Concept of a Creep-Hardening Surface", *International Journal of Solids and Structures*, Vol. 18, No. 7, pp. 597 – 609, (1982).
- [15] Ohno, N., "Recent Topics in Constitutive Modeling of Cyclic Plasticity and Viscoplasticity", *ASME Journal of Applied Mechanics Reviews*, Vol. 43, No. 11, pp. 283–295, (1990).
- [16] Lee, K.D., and Krempl, E., "An Orthotropic Theory of Viscoplasticity Based on Overstress for Thermomechanical Deformations", *International Journal of Solids and Structures*, Vol. 27, No. 11, pp. 1445–1459, (1991).
- [17] Shojaei, A., Eslami, M.R., and Mahbadi, H., "Cyclic Loading of Beams Based on the Chaboche Model", *International Journal of Mechanics and Materials in Design*, Vol. 6, No. 3, pp. 217-228, (2010).
- [18] Chaboche, J.L., "On Some Modifications of Kinematic Hardening to Improve the Description of Ratcheting Effects", *International Journal of Plasticity*, Vol. 7, No. 7, pp. 661-678, (1991).
- [19] Chaboche, J.L., "A Review of Some Plasticity and Viscoplasticity Constitutive Theories", *International Journal of Plasticity*, Vol. 105, pp. 1642-1693, (2008).
- [20] Mahbadi, H., and Eslami, M.R., "Load and Deformation Controlled Cyclic Loading of Beams Based on the Isotropic Hardening Model", *Transactions of Iranian Society of Mechanical Engineering*, Vol. 3, No. 1, pp. 28-46, (2002).
- [21] Mahbadi, H., and Eslami, M.R., "Load and Deformation Controlled Cyclic Loading of Thick Vessels Based on the Isotropic Hardening Model", *Transactions of Iranian Society of Mechanical Engineering*, Vol. 4, No. 1, pp. 5-25, (2003).

- [22] Mahbadi, H., Gowhari, A.R., and Eslami, M.R., "Elastic-Plastic-Creep Cyclic Loading of Beams using the Prager Kinematic Hardening Model", *IMechE Journal of Strain Analysis*, Vol. 39, No. 2, pp. 127-136, (2004).
- [23] Eslami, M.R., and Mahbadi, H., "Cyclic Loading of Thermal Stresses", *Journal of Thermal Stresses*, Vol. 24, No. 1, pp. 577-603, (2001).
- [24] Mahbadi, H., and Eslami, M.R., "Numerical Simulation of Cyclic Loading of Thermal Stresses", *Encyclopedia of Thermal Stresses*, Springer Netherlands, pp. 3434–3443. (2014).

Nomenclature

- a_1 : Material constant for Chaboche model
 a_2 : Material constant for Chaboche model
 b : Isotropic hardening material constant
 $2c$: Height of the beam
 h : Width of the beam
 n : Material constant for viscoplastic model
 C_1 : Material constant for Chaboche model
 C_2 : Material constant for Chaboche model
 E : Elastic modulus
 M : Bending moment
 P : Axial load
 Q : Isotropic hardening material constant

Greek symbols

- ϵ_x : Axial total strain
 ϵ_x^p : Axial plastic strain
 ϵ_x^{Res} : Axial residual strain
 σ_x : Axial stress
 σ_0 : Yield strength
 χ_{ij} : Backstress tensor

چکیده

در این مقاله، رفتار انباشتگی کرنش تیرها تحت بارهای مکانیکی در درجه حرارت‌های بالا، با استفاده از مدل یکپارچه ویسکوپلاستیک شاپوش با تئوری پلاستیسیته ترکیبی ایزوتروپیک و سینماتیک مورد بررسی قرار گرفته است. یک روند عددی جامع و دقیق بر پایه روش حل پیشرونده برای تعیین کرنش‌های غیرالاستیک خزش و پلاستیک پیشنهاد شده است. با اعمال روند عددی پیشنهادی بر معادلات بدست آمده از مدل یکپارچه ویسکوپلاستیک، رفتار سیکلی تیر در اثر ترکیب کرنش‌های پلاستیک و خزش مورد بررسی قرار گرفته است. تاثیر نرخ بارگذاری، کرنش خزش و بار متوسط بر دامنه تنش و رفتار انباشتگی کرنش تیر تحت ترکیب بارهای محوری و خمشی در درجه حرارت‌های بالا مورد مطالعه قرار گرفته است. نتایج نشان می‌دهند که افزایش نرخ بارگذاری منجر به کاهش نرخ انباشتگی کرنش و دامنه تنش می‌گردد. همچنین با افزودن زمان خزش، انباشتگی کرنش بیشتر و دامنه تنش کمتر شده است. نتایج این مقاله با داده‌های تجربی ارائه شده در سوابق علمی مقاله مقایسه شده است.